RAPID COMMUNICATION

Doping dependence of resistivity, upper critical field and its anisotropy in overdoped $Ba_{1-x}K_xFe_2As_2$ ($x = 0.6$–1) single crystals

Ke Shi(史可)[1,2], Wenshan Hong(洪文山)[3], Yang Li(李阳)[3,4], Minjie Zhang(张敏杰)[1,2], Yongqi Han(韩永琦)[1,2], Yu Zhao(赵宇)[1,2], Jiating Wu(吴嘉挺)[1,5], Ze Wang(王泽)[1], Langsheng Ling(凌浪生)[1], Chuanying Xi(郗传英)[1], Li Pi(皮雳)[1], Huiqian Luo(罗会仟)[3,†], and Zhaosheng Wang(王钊胜)[1,‡]

[1] *Anhui Key Laboratory of Low-Energy Quantum Materials and Devices, High Magnetic Field Laboratory, HFIPS, Chinese Academy of Sciences, Hefei* 230031, *China*

[2] *University of Science and Technology of China, Hefei* 230026, *China*

[3] *Beijing National Laboratory for Condensed Matter Physics, Institute of Physics, Chinese Academy of Sciences, Beijing* 100190, *China*

[4] *School of Physical Sciences, University of Chinese Academy of Sciences, Beijing* 100190, *China*

[5] *Electronic and Mechanical Engineering, Fujian Polytechnic Normal University, Fuzhou* 350300, *China*

(Received 11 October 2025; revised manuscript received 7 November 2025; accepted manuscript online 11 November 2025)

Temperature-dependent resistivity, upper critical field H_{c2} and its anisotropy in overdoped superconducting $Ba_{1-x}K_xFe_2As_2$ ($x = 0.6$–1) single crystals have been measured in steady magnetic fields up to 44 T and low temperatures down to 0.4 K. Analysis using both the quadratic term and power-law fitting demonstrates that the in-plane resistivity $\rho_{ab}(T)$ progressively approaches the Fermi-liquid T^2 behavior with increasing K doping and reaches a saturation plateau at $x \approx 0.8$. The temperature dependence of both H_{c2}^{ab} and H_{c2}^{c} follows the Werthamer–Helfand–Hohenberg model, incorporating orbital and spin paramagnetic effects. For $x \leq 0.8$, the orbital effect dominates for $H \parallel ab$, while the Pauli paramagnetic effect prevails for $H \parallel c$. For $x > 0.8$, the Pauli paramagnetic effect becomes dominant in both crystallographic directions. The anisotropy of $H_{c2}(0)$ exhibits a discontinuity in its dependence on K doping concentration with a significant enhancement at $x = 0.8$ and a maximum at $x = 0.9$. These experimental results indicate that the electron correlation effect is enhanced in the heavily overdoped $Ba_{1-x}K_xFe_2As_2$ system where the underlying symmetries are broken due to the Fermi surface reconstruction before $x = 0.9$.

Keywords: BaK122 single crystals, high magnetic fields, upper critical field H_{c2}, magnetoresistance

PACS: 74.25.Op, 74.25.F–, 74.70.Xa, 74.25.Dw

DOI: 10.1088/1674-1056/ae1df1 **CSTR:** 32038.14.CPB.ae1df1

1. Introduction

The upper critical field $H_{c2}(T)$ of type-II superconductors reveals fundamental properties such as pair-breaking mechanisms, Fermi surface anisotropy, and multiband effects. Within the framework of BCS theory, magnetic fields can suppress spin-singlet superconductivity either through the Zeeman effect, which disrupts spin-singlet pairing, or through orbital effects that modify electronic trajectories.[1,2] Iron-based superconductors exhibit significant potential for applications, particularly in high magnetic fields, owing to their exceptionally high H_{c2} and low anisotropy γ ($\gamma = H_{c2}^{ab}/H_{c2}^{c}$, typically ranging between 1 and 2).[3–8] Recent advancements in doping strategies and structural optimization have further enhanced the superconducting properties of these materials, facilitating their advancement toward practical applications.[7,9–12]

The 122-type iron-based superconductors crystallize in the $ThCr_2Si_2$-type tetragonal crystal structure, examples include AFe_2As_2 (A = Ba, Sr, Ca, Eu, K, Rb, and Cs)[13–18] and AFe_2Se_2 (A = Na, K, Rb, Cs, Tl, etc.).[19–22] The parent compounds of these materials (e.g., $BaFe_2As_2$) are non-superconducting in their pristine states, but superconductivity can be induced through chemical doping strategies involving electron doping, hole doping, isovalent doping, or pressure application.[15,23–27] Co-doped $BaFe_2As_2$ single crystals exhibit superconductivity with an onset superconducting transition temperature of 22 K.[24] Similarly, $BaFe_{2-x}Ni_xAs_2$ single crystals with electron-dominated carriers exhibit a superconducting transition temperature of 20 K under optimal doping.[25] Substitution of Ba with K enables the synthesis of hole-doped superconductors.[15] In contrast to electron-doped systems, the hole-doped $BaFe_2As_2$ system exhibits a higher T_c and more complex phase diagram, providing a platform for investigating the interplay among multiple phases in iron-based superconductors.[15,26]

In the $Ba_{1-x}K_xFe_2As_2$ system, hole doping via K substitution progressively suppresses the Néel temperature T_N, leading to its full disappearance near the critical doping level $x \approx 0.25$.[23,28,29] Superconductivity emerges at $x = 0.1$, reaches a maximum critical temperature T_c of approx-

†Corresponding author. E-mail: hqluo@iphy.ac.cn

‡Corresponding author. E-mail: zswang@hmfl.ac.cn

imately 38 K near $x = 0.4$, and subsequently decreases in the overdoped region while persisting up to $x = 1$.[15,28–32,34] It has been reported that underdoped systems exhibit an exceptionally high upper critical field accompanied by a remarkably low superconducting anisotropy ratio.[32,33] Optimally doped $Ba_{0.6}K_{0.4}Fe_2As_2$ exhibits an upper critical field exceeding 60 T, and its unique Fermi surface topology results in orbital-limited upper critical fields across all magnetic field orientations.[35] However, at higher doping levels, $Ba_{1-x}K_xFe_2As_2$ exhibits a deviation from the universal trend observed in iron-based superconductors.[36–39] Specifically, in the composition range of $0.7 \leq x \leq 0.8$, it exhibits a novel bosonic metallic state characterized by spontaneous time-reversal symmetry breaking.[36,40,41] Further increasing K doping, theoretical calculations based on density functional theory (DFT) by Khan *et al.* predicted a Lifshitz transition at $x \approx 0.9$,[37] which was subsequently confirmed experimentally in the heavily overdoped regime.[37,42,43] Notably, at the extreme end of doping ($x = 0.95$), specific heat measurements on $Ba_{0.05}K_{0.95}Fe_2As_2$ reveal a three-component superconducting order parameter and a linear magnetic field dependence of the specific heat coefficient, indicating the dominant role of the Pauli-limiting effect.[44] At full substitution, KFe_2As_2 is a superconductor exhibiting solely hole-like Fermi surfaces and strong electron correlations,[38] and angle-resolved photoemission spectroscopy (ARPES) measurements have confirmed it to be a anisotropic s±-wave superconductor,[45] demonstrating that even a compound possessing exclusively hole-type Fermi surfaces exhibits the same gap symmetry as systems with both hole- and electron-type Fermi surfaces.[45]

In this paper, we report a systematic study of the temperature-dependent in-plane resistivity, H_{c2} and its anisotropy in overdoped $Ba_{1-x}K_xFe_2As_2$ ($x = 0.6$–1) single crystals. Measurements were performed in steady magnetic fields up to 44 T and at temperatures down to 0.4 K. The in-plane resistivity $\rho_{ab}(T)$ progressively approaches the Fermi-liquid T^2 behavior with increasing K doping. Based on the Werthamer–Helfand–Hohenberg (WHH) model, the $H_{c2}(0)$ shows a monotonic decrease, while the zero-temperature anisotropy parameter $\gamma(0)$ increases from 1.5 to 2.5 with increasing K concentration. Analysis of the resistivity fitting parameters, combined with the evolution trends of $H_{c2}(T)$ and $\gamma(0)$ with K doping, reveals that the superconductivity in the overdoped $Ba_{1-x}K_xFe_2As_2$ system undergoe a transition in the correlation length within the doping range $x = 0.8$–0.9. Beyond this range, the electronic correlation effects become significantly enhanced, which is probably related to the anisotropic gaps in KFe_2As_2.

2. Experiment

The $Ba_{1-x}K_xFe_2As_2$ ($x = 0.6$–1) single crystals were grown using the self-flux method with FeAs as the flux. Details regarding crystal growth and characterization are described in Refs. [31,39]. The doping concentration was determined based on the T_c values from the phase diagram of this system in Refs. [40,46]. Figure 1(b) illustrates the position of our samples in the phase diagram. The temperature dependence of the in-plane resistivity under various magnetic fields — applied parallel to the *ab* plane ($H \parallel ab$) and along the *c* axis ($H \parallel c$) — was measured using the standard four-probe method. These measurements were performed at the Steady High Magnetic Field Facilities, Chinese Academy of Sciences,[47] where temperatures down to 0.4 K and magnetic fields up to 44 T using the hybrid magnet were achieved. A constant current of 1 mA was applied, with the current direction maintained perpendicular to the applied magnetic field throughout the measurements.

3. Results and discussion

Figure 1(a) presents the in-plane resistivity of five samples with different doping concentrations in zero field up to 300 K. In order to minimize the influence of size effects and facilitate the comparison of the variation of the curves, the resistivity was normalized ($\tilde{\rho} = \rho_{ab}(T)/\rho_{ab}(300\ \mathrm{K})$). For clarity, the curves have been offset vertically. As shown, all the curves display very similar behavior in the normal state. It is clear that K doping completely suppresses the AF/structural

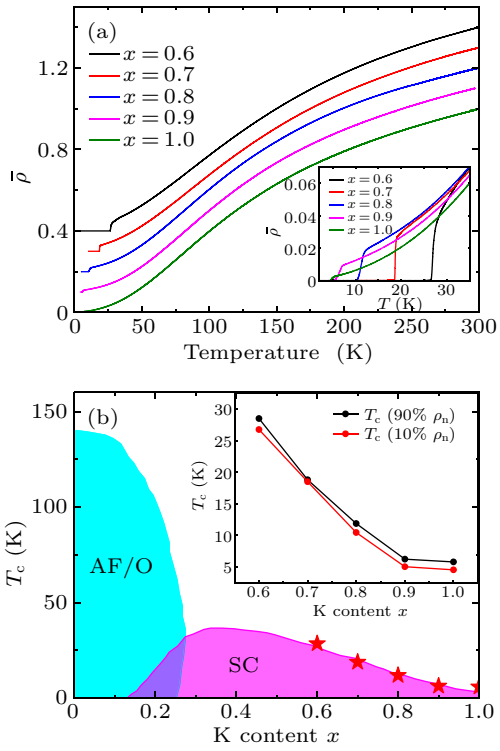

Fig. 1. (a) Temperature dependence of the normalized resistivity $\tilde{\rho} = \rho_{ab}(T)/\rho_{ab}(300\ \mathrm{K})$ in zero field up to 300 K for $Ba_{1-x}K_xFe_2As_2$ ($x = 0.6$–1) single crystals. The data for each doping are offset vertically by 0.1 for clarity. The inset is an enlarged graph around the superconducting transition. (b) Location of our samples (red stars) in $Ba_{1-x}K_xFe_2As_2$ phase diagram. The diagram is adapted from Ref. [46]. The inset of (b) is the doping dependence of T_c for $Ba_{1-x}K_xFe_2As_2$ ($x = 0.6$–1) single crystals.

phase transition in the system. All samples exhibit very narrow superconducting transition widths, indicating high crystal quality. The inset of Fig. 1(b) shows the T_c values for different K-doping levels. The T_c, defined as the temperature corresponding to 90% of the normal-state resistivity value, are approximately 28.5 K, 18.8 K, 11.9 K, 6.3 K, and 5.8 K for different doping levels.

3.1. Doping evolution of the temperature-dependent resistivity

Figure 2(a) displays the temperature dependence of the normalized resistivity $\bar{\rho}$ for the five samples with different doping levels, measured in zero magnetic field up to 100 K. The data reveal that the nonlinearity of the ρ–T curve becomes increasingly pronounced at low temperatures. To precisely characterize the evolution of the resistivity's temperature dependence with doping, we fit the data in the temperature range from $T_c + 5$ K to 60 K using a second order polynomial function[48]

$$\bar{\rho} = \alpha_0 + \alpha_1 T + \alpha_2 T^2, \tag{1}$$

where α_0, α_1, α_2 are the fitting parameters. Figures 2(b)–2(d) display the variation of these parameters with increasing K doping level. It is clear that the magnitude of the linear term α_1 progressively diminishes with higher K doping, while the quadratic term α_2 becomes more prominent.

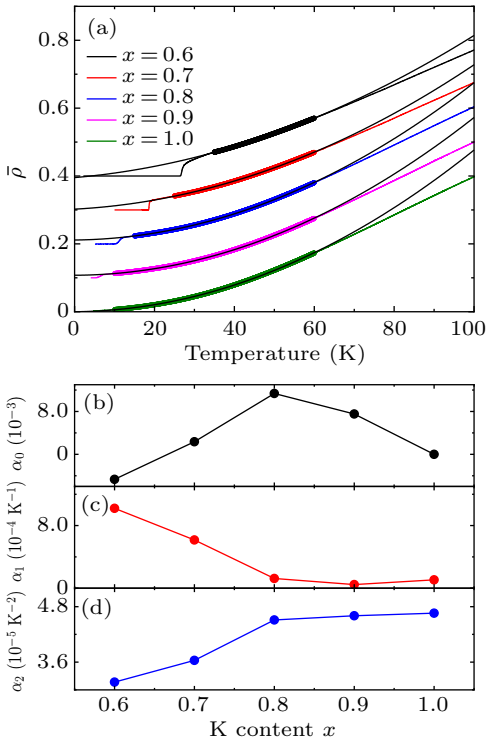

Fig. 2. (a) Fitting of the temperature-dependent in-plane normalized resistivity $\bar{\rho}$ for $Ba_{1-x}K_xFe_2As_2$ ($x = 0.6$–1) with the second-order polynomial. The data for each doping are offset vertically by 0.1 for clarity. (b), (c) and (d) The fitting parameters α_0, α_1 and α_2 for five different doping levels.

The power-law relationship can also be employed to model the observational data:

$$\bar{\rho} = \rho_0 + AT^n, \tag{2}$$

with three fitting parameters ρ_0, A, and n for each curve. Figure 3(a) displays the logarithmic plot derived from this power function, where the fitted curve exhibits a slope of n and a Y-axis intercept of $\log A$. For comparison, power-law analysis was also performed over the temperature range from $T_c + 5$ K to 60 K. The resulting fitting parameters A and n are shown in Figs. 3(b) and 3(c), respectively. As K doping increases, the coefficient A of the power-law term continuously decreases, while the power-law exponent n asymptotically approaches 2. It is evident that both fitting results converge towards the Fermi-liquid T^2 dependence. A maximum deviation from this T^2 dependence has been observed at the optimal doping $x = 0.4$,[49,50] suggesting the presence of a possible quantum critical point.[28]

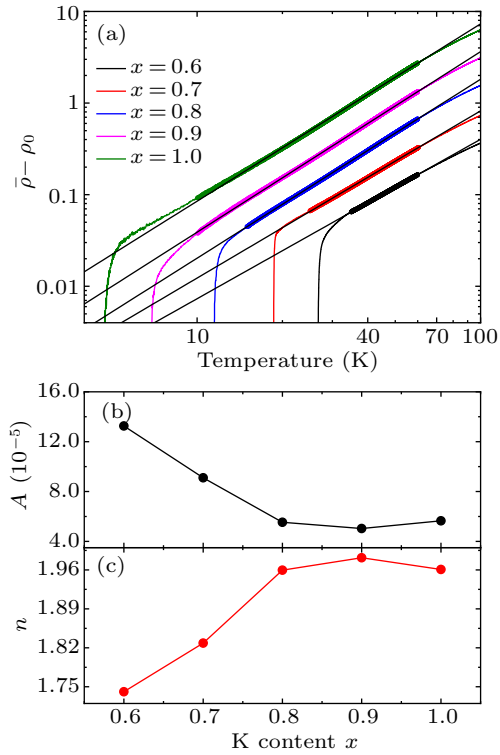

Fig. 3. (a) Fitting of the temperature-dependent in-plane normalized resistivity $\bar{\rho}$ for $Ba_{1-x}K_xFe_2As_2$ ($x = 0.6$–1) with the power-law function. The data for each doping are offset vertically by 0.3 for clarity. (b) and (c) The fitting parameters A and n for five different doping levels.

It has been reported that there is a scaling law between T_c and the T-linear resistivity coefficient in cuprates and FeSe in the strange-metal region.[51,52] However, Figs. 2 and 3 show that the doping evolution of parameters α_1 and α_2 (from quadratic fitting) and parameters A and n (from power-law fitting) exhibit saturation within the doping range $x = 0.8$–1. This saturation coincides with evidence from thermoelectric power and Hall coefficient measurements indicating the occurrence of a Lifshitz transition in this range.[53,54] According

to the Kadowaki–Woods relation (KWR),[55] the quadratic coefficient in the low-temperature ρ–T fitting function is proportional to the square of the quasiparticle effective mass (m^{*2}). Furthermore, the ratio of α_2 to the square of the electronic specific heat coefficient is a constant. Deviation of this constant from its standard value is regarded as an indicator of strong electron correlations.[55] Strong electron correlations have been established in KFe_2As_2.[38] For the five samples in this study, the increase in the quadratic coefficient with K-doping level signifies an enhancement of electron–electron correlations within the system. The observed saturation indicates that the strength of these electron correlations has reached a relatively stable regime.

3.2. Doping evolution of the anisotropic upper critical fields

Figure 4 displays the temperature and magnetic-field dependent resistivity $\rho_{ab}(T)$ curves of the $Ba_{0.4}K_{0.6}Fe_2As_2$ single crystal at magnetic fields up to 44 T parallel to the *ab* planes and along the *c* axis, respectively. For the five samples, the magnetic field induces a parallel shift of the resistive transition curves toward lower temperatures, suggesting the presence of field-induced pair-breaking effects in this system. This behavior contrasts sharply with that observed in cuprate superconductors, where the resistive transition $\rho(T)$ broadens due to the formation of a fan-like structure, while the onset region remains largely unaffected by changes in the magnetic field.[56,57]

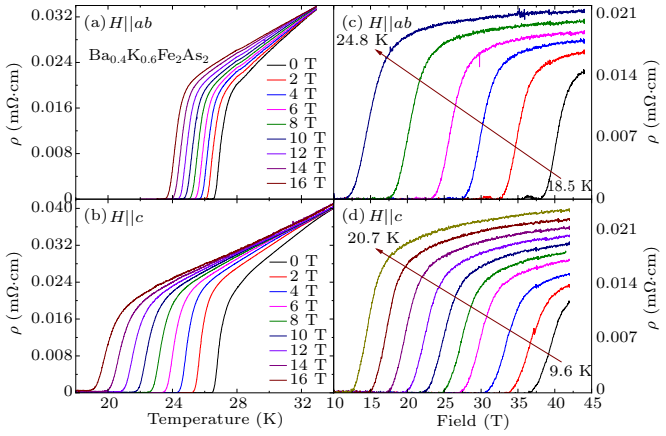

Fig. 4. (a) and (b) The temperature dependence of the in-plane resistivity ρ_{ab} in single crystal of $Ba_{0.4}K_{0.6}Fe_2As_2$ with $H \parallel ab$ and $H \parallel c$ measured in a superconducting magnet up to 16 T. (c) and (d) The magnetic field dependence of the in-plane resistivity ρ_{ab} in single crystal of $Ba_{0.4}K_{0.6}Fe_2As_2$ with $H \parallel ab$ (T = 18.5 K, 20.1 K, 21.5 K, 22.6 K, 23.8 K, 24.8 K) and $H \parallel c$ (T = 9.6 K, 11.0 K, 12.4 K, 13.7 K, 14.8 K, 16.0 K, 17.2 K, 18.4 K, 19.5 K, 20.7 K) measured in a hybrid magnet up to 44 T.

The temperature dependence of H_{c2}^{ab} and H_{c2}^{c} for the five samples with x = 0.6–1 is shown in Fig. 5 (where $H_{c2}(T)$ is defined at $\rho = 90\%\rho_n$). Solid symbols represent data obtained from field scans, while open symbols denote data from temperature scans. Analysis of the low-temperature resistivity fitting curves (presented earlier) indicates a gradual strengthening of electronic correlations in the x = 0.6–0.8 samples. For the x = 0.8 samples, $H_{c2}^{ab}(T)$ exhibits a tendency towards saturation with decreasing temperature, whereas $H_{c2}^{c}(T)$ shows a quasi-linear increase with no discernible saturation at low temperatures. The Pauli-limiting field for a weakly coupled BCS superconductor in the absence of spin–orbit scattering is estimated as[58] $H_P^{BCS}(0) = 1.86T_c$ = 22.1 T for the $Ba_{0.2}K_{0.8}Fe_2As_2$ sample (T_c = 11.9 K). Alternatively, the orbital limiting field is given by the WHH formula $H_{c2}^{orb}(0) = -0.69\,dH_{c2}/dT|_{T=T_c}T_c$.[59] For the x = 0.8 samples, the slopes dH_{c2}/dT are −4.07 T/K for $H \parallel ab$ and −1.39 T/K for $H \parallel c$, yielding $H_{c2}^{orb,ab}(0)$ = 33.5 T and $H_{c2}^{orb,c}(0)$ = 11.5 T. These estimates disagree with our experimental data. The discrepancies between the theoretical estimates and experimental data are frequently observed in iron-based superconductors.[7,8,32,60] This discrepancy arises because the formula, rooted in isotropic s-wave superconductors, neglects spin–orbit coupling and Pauli paramagnetic effects.

In contrast, the WHH model incorporates the Maki parameter α and the spin–orbit scattering constant λ_{so}, enabling a more precise description of the experimentally observed temperature-dependent behavior of H_{c2}:[59]

$$\ln\left(\frac{1}{t}\right) = \sum_{\nu=-\infty}^{\infty}\left(\frac{1}{|2\nu+1|} - \left[|2\nu+1| + \frac{\bar{h}}{t} + \frac{(\alpha\bar{h}/t)^2}{|2\nu+1| + (\bar{h}+\lambda_{so})/t}\right]^{-1}\right), \tag{3}$$

where $t = T/T_c$ and $\bar{h} = (4/\pi^2)\left[H_{c2}(T)/|dH_{c2}/dT|_{T_c}\right]$. As shown in Figs. 5(a) and 5(b), the best fit using this model reproduces both of the experimental H_{c2}^{ab} and H_{c2}^{c} data very well for all five samples (all fit parameters are listed in Table 1). In contrast, previously reported iron-based superconductors generally require a two-band model to fit H_{c2}^{c}, such as Co/Ni-doped iron-based superconductors.[34,60–62] For x = 0.8, we obtain H_{c2}^{ab} = 22.2 T (α = 2.5 and λ_{so} = 1.5) and H_{c2}^{c} = 13.3 T (α = 0.5 and λ_{so} = 4). The results indicate that for samples with $x \le 0.8$, the orbital effect mechanism dominates for $H \parallel ab$, while the Pauli effect prevails for $H \parallel c$. For $x > 0.8$, the Pauli effect becomes dominant in both crystallographic directions (Fig. 5(b)). The temperature dependence of the anisotropic γ for x = 0.8 is shown in Fig. 6(a). The γ parameter exhibits a monotonically increasing trend with rising temperature, whereas in Co-doped electron-type superconductors, the temperature dependence of γ displays a peak near T_c.[63] In the overdoped $BaFe_{2-x}Ni_xAs_2$ superconductor, $\gamma(0)$ exhibits a monotonic increase with doping concentration,[60] whereas the overdoped $Ba_{1-x}K_xFe_2As_2$ samples display distinct behavior. As shown in Fig. 6(b), there is a pronounced anomaly in $\gamma(0)$ within the range of x = 0.8–0.9. It can be attributed to a saturation of the enhanced electron correlation strength

in this regime, where the system evolves into a strongly correlated metallic state after the Lifshitz transition at $x = 0.9$, and the superconducting gaps become strongly anisotropic in KFe_2As_2 ($x = 1$). However, it is not clear whether the time-reversal symmetry breaking can trigger the enhancement of electron correlations. Further investigations on the detailed doping dependence of the band structure are necessary to clarify this issue.

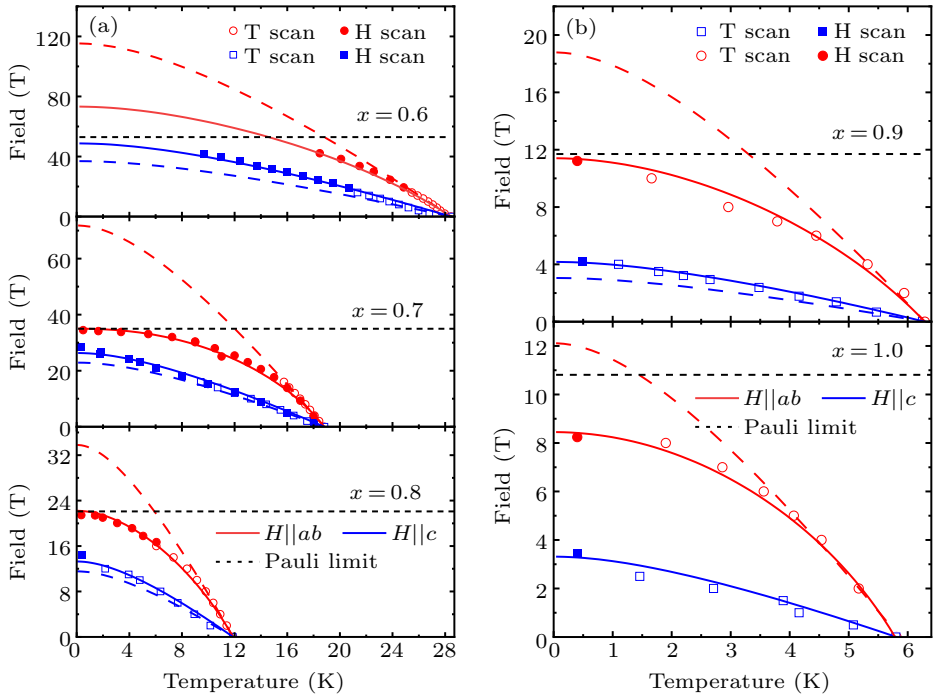

Fig. 5. Temperature dependence of H_{c2} of the five overdoped samples extracted from the magnetotransport measurements. (a) $x = 0.6$, 0.7, 0.8. (b) $x = 0.9$, 1.0. The solid symbols are obtained from H-scan measuremengts, and the open symbols are obtained from T-scan measurements. The solid lines show a WHH fit with the parameter α and λ_{so} as given in Table 1 for both H_{c2}^{ab} and H_{c2}^{c}. The dotted lines are the WHH predictions with $\alpha = 0$ and $\lambda_{so} = 0$ for both H_{c2}^{ab} and H_{c2}^{c}. The black dashed lines show the Pauli limit.

Table 1. Summary of the parameters for the upper critical field for all investigated compositions of $Ba_{1-x}K_xFe_2As_2$.

x	T_c (K)	$-dH_{c2}^{ab}/dT$ (T/K)	$-dH_{c2}^{c}/dT$ (T/K)	$H_{c2}^{orb,ab}(0)$ (T)	$H_{c2}^{orb,c}(0)$ (T)	$H_P^{BCS}(0)$ (T)	α^{ab}	λ_{so}^{ab}	α^{c}	λ_{so}^{c}	$H_{c2}^{ab}(0)$ (T)	$H_{c2}^{c}(0)$ (T)	$\gamma(0)$
0.6	28.5	5.29	1.84	116.3	36.3	52.9	3.5	3	1	5	73.4	48.9	1.51
0.7	18.8	5.52	1.74	71.9	22.7	35.0	3.3	0.5	0.3	3	35.1	25.6	1.32
0.8	11.9	4.07	1.39	33.5	11.5	22.1	2.5	1.5	0.5	4	22.2	13.3	1.67
0.9	6.3	4.31	0.7	18.8	3.0	11.7	2.5	1	1	5	11.4	4.2	2.75
1.0	5.8	2.98	0.84	12.1	3.4	10.8	3.1	0.8	0	0	8.5	3.3	2.57

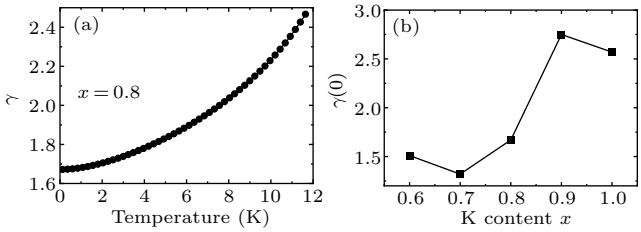

Fig. 6. (a) The temperature dependence of the anisotropy γ for $x = 0.8$ sample. (b) The anisotropy parameter $\gamma(0)$ of the five samples calculated from the WHH fitting results.

4. Conclusion

The temperature-dependent resistivity, upper critical field H_{c2} and its anisotropy in overdoped superconducting $Ba_{1-x}K_xFe_2As_2$ ($x = 0.6$–1) single crystals have been determined at high magnetic fields up to 44 T and low temperatures down to 0.4 K. Analysis using both the quadratic term and power-law fitting demonstrates that the in-plane resistivity $\rho_{ab}(T)$ progressively approaches the Fermi-liquid T^2 behavior with increasing K doping and reaches a saturation plateau at $x \approx 0.8$. The temperature dependence of both H_{c2}^{ab} and H_{c2}^{c} can be well described by the WHH model incorporating orbital and Pauli paramagnetic limiting effects. The zero-temperature upper critical field, $H_{c2}(0)$, decreases monotonically with increasing K doping. For $x \leq 0.8$, orbital limiting dominates for $H \parallel ab$, while Pauli limiting prevails for $H \parallel c$. For $x > 0.8$, Pauli limiting becomes dominant for both field orientations. The $\gamma(0)$ exhibits an abrupt change within the doping range $x = 0.8$–0.9. These findings demonstrate that the superconductivity in the overdoped $Ba_{1-x}K_xFe_2As_2$ is highly sensitive to the Fermi surface topology and band structure in the range $x = 0.8$–0.9. Upon exceeding this doping range, electron correlations are markedly enhanced, driving the system into a strongly correlated metallic state.

Acknowledgements

This work was supported by the National Key Research and Development Program of China (Grant Nos. 2024YFA1611100, 2023YFA1406100, and 2018YFA0704201), the Systematic Fundamental Research Program Leveraging Major Scientific and Technological Infrastructure, Chinese Academy of Sciences (Grant No. JZHKYPT-2021–08), the National Natural Science Foundation of China (Grant Nos. 11704385, 11874359, and 12274444), the Strategic Priority Research Program (B) of the Chinese Academy of Sciences (Grant No. XDB25000000), and Steady High Magnetic Field Facility Instrument and Equipment Renovation. We thank the Magnetic Property Measurement System (https://cstr.cn/31125.02.SHMFF.MPMS) and HM1 (https://cstr.cn/31125.02.SHMFF.HM) at the Steady High Magnetic Field Facility, CAS (https://cstr.cn/31125.02.SHMFF), for providing technical support and assistance in data collection and analysis.

References

[1] Bardeen J, Cooper L N and Schrieffer J R 1957 *Phys. Rev.* **108** 1175
[2] Matsuda Y and Shimahara H 2007 *J. Phys. Soc. Jap.* **76** 051005
[3] Hunte F, Jaroszynski J, Gurevich A, Larbalestier D C, Jin R, Sefat A S, McGuire M A, Sales B C, Christen D K and Mandrus D 2008 *Nature* **453** 903
[4] Senatore C, Flükiger R, Cantoni M, Wu G, Liu R H and Chen X H 2008 *Phys. Rev. B* **78** 054514
[5] Jia Y, Cheng P, Fang L, Luo H, Yang H, Ren C, Shan L, Gu C and Wen H H 2008 *Appl. Phys. Lett.* **93** 032503
[6] Tarantini C, Gurevich A, Jaroszynski J, Balakirev F, Bellingeri E, Pallecchi I, Ferdeghini C, Shen B, Wen H H and Larbalestier D C 2011 *Phys. Rev. B* **84** 184522
[7] Shi K, Zhang M J, Han Y Q, Zhao Y, Wang Z, Ling L S, Tong W, Xi C Y, Pi L, Ni S L, Zhou, M H and Wang Z S 2025 *Supercond. Sci. Tech.* **38** 055023
[8] Khim S, Kim J W, Choi E S, Bang Y, Nohara M, Takagi H and Kim K H 2010 *Phys. Rev. B* **81** 184511
[9] Zhang M, Wu J, Shi K, Ling L, Tong W, Xi C, Pi L, Wosnitza J and Luo H 2023 *Appl. Phys. Lett.* **123** 072602
[10] Chen Z W, Zhang Y, Ma P, Xu Z T, Li Y L, Wang Y, Lu J M, Ma Y W and Gan Z Z 2024 *Chin. Phys. B* **33** 047405
[11] Huang Y N, Ye Z F, Liu D Y and Qiu H Q 2024 *Chin. Phys. Lett.* **40** 097405
[12] Zeng W J, Zhang Z Y, Dong X Y, Tu Y B, Wu Y W, Wang T, Zhang F, Shao S, Hou J, Hou X Y, Hao N, Mu G and Shan L 2025 *Chin. Phys. B* **34** 087402
[13] Lee S, Jiang J, Zhang Y, Bark C W, Weiss J D, Tarantini C, Nelson C T, Jang H W, Folkman C M, Baek S H, Polyanskii A, Abraimov D, Yamamoto A, Park J W, Pan X Q, Hellstrom E E, Larbalestier D C and Eom C B 2010 *Nat. Mater.* **9** 397
[14] Choi E M, Jung S G, Lee N H, Kwon Y S, Kang W N, Kim D H, Jung M H, Lee S I and Sun L 2009 *Appl. Phys. Lett.* **95** 062507
[15] Sasmal K, Lv B, Lorenz B, Guloy A M, Chen F, Xue Y Y and Chu C W 2008 *Phys. Rev. Lett.* **101** 107007
[16] Rotter M, Tegel M and Johrendt D 2008 *Phys. Rev. Lett.* **101** 107006
[17] Wu G, Chen H, Wu T, Xie Y L, Yan Y J, Liu R H, Wang X F, Ying J J and Chen X H 2008 *J. Phys.: Condens. Matter* **20** 422201
[18] Ronning F, Klimczuk T, Bauer E D, Volz H and Thompson J D 2008 *J. Phys.: Condens. Matter* **20** 322201
[19] Guo J, Jin S, Wang G, Wang S, Zhu K, Zhou T, He M and Chen X 2010 *Phys. Rev. B* **82** 180520
[20] Krzton-Maziopa A, Shermadini Z, Pomjakushina E, Pomjakushin V, Bendele M, Amato A, Khasanov R, Luetkens H and Conder K 2011 *J. Phys.: Condens. Matter* **23** 052203
[21] Wang A F, Ying J J, Yan Y J, Liu R H, Luo X G, Li Z Y, Wang X F, Zhang M, Ye G J, Cheng P, Xiang Z J and Chen X H 2011 *Phys. Rev. B* **83** 060512
[22] Fang M H, Wang H-D, Dong C H, Li Z J, Feng C M, Chen J and Yuan H Q 2011 *Europhys. Lett.* **94** 27009
[23] Rotter M, Tegel M, Johrendt D, Schellenberg I, Hermes W and Pöettgen R 2008 *Phys. Rev. B* **78** 020503
[24] Sefat A S, Jin R, McGuire M A, Sales B C, Singh D J and Mandrus D 2008 *Phys. Rev. Lett.* **101** 117004
[25] Li L J, Luo Y K, Wang Q B, Chen H, Ren Z, Tao Q, Li Y K, Lin X, He M, Zhu Z W, Cao G H and Xu Z A 2009 *New J. Phys.* **11** 025008
[26] Aswartham S, Abdel-Hafiez M, Bombor D, Kumar M, Wolter A U B, Hess C, Evtushinsky D V, Zabolotnyy V B, Kordyuk A A, Kim T K, Borisenko S V, Behr G, Büchner B and Wurmehl S 2012 *Phys. Rev. B* **85** 224520
[27] Qiu X, Zhou S Y, Zhang H, Pan B Y, Hong X C, Dai Y F, Eom M J, Kim J S, Ye Z R, Zhang Y, Feng D L and Li S Y 2012 *Phys. Rev. X* **2** 011010
[28] Shen B, Yang H, Wang Z S, Han F, Zeng B, Shan L, Ren C and Wen H H 2011 *Phys. Rev. B* **84** 184512
[29] Rotter M, Pangerl M, Tegel M and Johrendt D 2008 *Angew. Chem. Int. Ed.* **47** 7949
[30] Li Z, Zhou R, Liu Y, Sun D L, Yang J, Lin C T and Zheng G Q 2012 *Phys. Rev. B* **86** 180501
[31] Luo H, Wang Z, Yang H, Cheng P, Zhu X and Wen H H 2008 *Supercond. Sci. Tech.* **21** 125014
[32] Wang Z S, Luo H Q, Ren C and Wen H H 2008 *Phys. Rev. B* **78** 140501
[33] Tanatar M A, Liu Y, Jaroszynski J, Brooks J S, Lograsso T A and Prozorov R 2017 *Phys. Rev. B* **96** 184511
[34] Zocco D A, Grube K, Eilers F, Wolf T and Löhneysen H V 2013 *Phys. Rev. Lett.* **111** 057007
[35] Yuan H Q, Singleton J, Balakirev F F, Baily S A, Chen G F, Luo J L and Wang N L 2009 *Nature* **457** 565
[36] Shipulin I, Stegani N, Maccari I, Kihou K, Lee C H, Hu Q X, Zheng Y, Yang F Z, Li Y W, Yim C M, Hühne R, Klauss H H, Putti M, Caglieris F, Babaev E and Grinenko V 2023 *Nat. Commun.* **14** 6374
[37] Khan S N and Johnson D D 2014 *Phys. Rev. Lett.* **112** 156401
[38] Hardy F, Böhmer A E, Aoki D, Burger P, Wolf T, Schweiss P, Heid R, Adelmann P, Yao Y X, Kotliar G, Schmalian J and Meingast C 2013 *Phys. Rev. Lett.* **111** 027002
[39] Li Y, Wu D, Shu Y, Liu B, Stuhr U, Deng G, Stampfl A P J, Zhao L, Zhou X, Li S, Pokhriyal A, Ghosh H, Hong W and Luo H 2025 *Chin. Phys. Lett.* **42** 067405
[40] Grinenko V, Sarkar R, Kihou K, Lee C H, Morozov I, Aswartham S, Büchner B, Chekhonin P, Skrotzki W, Nenkov K, Hühne R, Nielsch K, Drechsler S L, Vadimov V L, Silaev M A, Volkov P A, Eremin I, Luetkens H and Klauss H H 2020 *Nat. Phys.* **16** 789
[41] Grinenko V, Weston D, Caglieris F, Wuttke C, Hess C, Gottschall T, Maccari I, Gorbunov D, Zherlitsyn S, Wosnitza J, Rydh A, Kihou K, Lee C H, Sarkar R, Dengre S, Garaud J, Charnukha A, Hühne R, Nielsch K, Büchner B, Klauss H H and Babaev E 2021 *Nat. Phys.* **17** 1254
[42] Tafti F F, Juneau-Fecteau A, Delage M È, de Cotret S R, Reid J P, Wang A F, Luo X G, Chen X H, Doiron-Leyraud N and Taillefer L 2013 *Nat. Phys.* **9** 349
[43] Bud'ko S L, Sturza M, Chung D Y, Kanatzidis M G and Canfield P C 2013 *Phys. Rev. B* **87** 100509
[44] Zhang S, Singh Y P, Huang X Y, Chen X J, Dzero M and Almasan C C 2015 *Phys. Rev. B* **92** 174524
[45] Wu D, Jia J, Yang J, Hong W, Shu Y, Miao T, Yan H, Rong H, Ai P, Zhang X, Yin C, Liu J, Chen H, Yang Y, Peng C, Li C, Zhang S, Zhang F, Yang F, Wang Z, Zong N, Liu L, Li R, Wang X, Peng Q, Mao H, Liu G, Li S, Chen Y, Luo H, Wu X, Xu Z, Zhao L and Zhou X J 2024 *Nat. Phys.* **20** 571
[46] Avci S, Chmaissem O, Chung D Y, Rosenkranz S, Goremychkin E A, Castellan J P, Todorov I S, Schlueter J A, Claus H, Daoud-Aladine A, Khalyavin D D, Kanatzidis M G and Osborn R 2012 *Phys. Rev. B* **85** 184507
[47] Fang Z, Chen W G, Huang P C, Chen Z Y, Ding H W, Zhao H, Qian X X, Jiang S L, Zhang Y and Kuang G L 2024 *IEEE Trans. Appl. Supercond.* **34** 1
[48] Doiron-Leyraud N, Auban-Senzier P, de Cotret S R, Bourbonnais C, Jérome D, Bechgaard K and Taillefer L 2009 *Phys. Rev. B* **80** 214531

[49] Liu Y, Tanatar M A, Straszheim W E, Jensen B, Dennis K W, McCallum R W, Kogan V G, Prozorov R and Lograsso T A 2014 *Phys. Rev. B* **89** 134504

[50] Shen B, Yang H, Wang Z S, Han F, Zeng B, Shan L, Ren C and Wen H H 2011 *Phys. Rev. B* **84** 184512

[51] Yuan J, Chen Q, Jiang K, Feng Z, Lin Z, Yu H, He G, Zhang J, Jiang X, Zhang X, Shi Y, Zhang Y, Qin M, Cheng Z G, Tamura N, Yang Y, Xiang T, Hu J, Takeuchi I, Jin K and Zhao Z 2022 *Nature* **602** 431

[52] Jiang X, Qin M, Wei X, Xu L, Ke J, Zhu H, Zhang R, Zhao Z, Liang Q, Wei Z, Lin Z, Feng Z, Chen F, Xiong P, Yuan J, Zhu B, Li Y, Xi C, Wang Z, Yang M, Wang J, Xiang T, Hu J, Jiang K, Chen Q, Jin K and Zhao Z 2023 *Nat. Phys.* **19** 365

[53] Hodovanets H, Liu Y, Jesche A, Ran S, Mun E D, Lograsso T A, Bud'ko S L and Canfield P C 2014 *Phys. Rev. B* **89** 224517

[54] Liu Y and Lograsso T A 2014 *Phys. Rev. B* **90** 224508

[55] Jacko A C, Fjærestad J O and Powell B J 2009 *Nat. Phys.* **5** 422

[56] Carrington A, Mackenzie A P, Sinclair D C and Cooper J R 1994 *Phys. Rev. B* **49** 13243

[57] Fuchs D T, Zeldov E, Rappaport M, Tamegai T, Ooi S and Shtrikman H 1998 *Nature* **391** 373

[58] Clogston A M 1962 *Phys. Rev. Lett.* **9** 266

[59] Helfand E and Werthamer N R 1966 *Phys. Rev.* **147** 288

[60] Wang Z, Xie T, Kampert E, Förster T, Lu X, Zhang R, Gong D, Li S, Herrmannsdörfer T, Wosnitza J and Luo H 2015 *Phys. Rev. B* **92** 174509

[61] Bristow M, Gower A, Prentice J C A, Watson M D, Zajicek Z, Blundell S J, Haghighirad A A, McCollam A and Coldea A I 2023 *Phys. Rev. B* **108** 184507

[62] Jaroszynski J, Hunte F, Balicas L, Jo Y, Raićević I, Gurevich A, Larbalestier D C, Balakirev F F, Fang L, Cheng P, Jia Y and Wen H H 2008 *Phys. Rev. B* **78** 174523

[63] Vinod K, Satya A T, Sharma Shilpam, Sundar C S and Bharathi A 2011 *Phys. Rev. B* **84** 012502